1-1-2017

New ages for the Upper Palaeolithic site of Xibaimaying in the Nihewan Basin, northern China: implications for small-tool and microblade industries in north-east Asia during Marine Isotope Stages 2 and 3

Yujie Guo
Peking University, yg991@uowmail.edu.au

Bo Li
University of Wollongong, bli@uow.edu.au

Jia-Fu Zhang
Peking University

Bao Yin Yuan
Chinese Academy Of Sciences

Fei Xie
Cultural Relics Of Hebei Province

See next page for additional authors

New ages for the Upper Palaeolithic site of Xibaimaying in the Nihewan Basin, northern China: implications for small-tool and microblade industries in north-east Asia during Marine Isotope Stages 2 and 3

Abstract
It has been suggested that the 'small-tool' and microblade Upper Palaeolithic industries coexisted in the Nihewan Basin of northern China for about 8-14 000 years during Marine Isotope Stage (MIS) 2. This inference was based on uranium-series ages of around 15 and 18 ka for bovid teeth recovered from the 'latest' small-tool site of Xibaimaying - the youngest occurrence of such tools in the region - and optically stimulated luminescence (OSL) dating of the earliest typical microblade site (Youfang: ~26-29 ka). In this study, we re-dated the Xibaimaying site using single-grain OSL methods and the resulting ages indicate that the cultural layer was deposited 46 ± 3 ka ago, during MIS 3 - more than 20 millennia earlier than previously thought and older also than the so-called earliest 'primitive' and typical microblade tools found at Zhiyu (~31-39 ka cal BP) and Youfang. These new ages for human occupation of Xibaimaying remove support for the parallel development of the small-tool and microblade industries in the Nihewan Basin during the Upper Palaeolithic, but reliable age estimates from additional sites are needed to confidently infer the nature of the chronological relationship between these two Upper Palaeolithic industries and the associated toolmakers.

Disciplines
Medicine and Health Sciences | Social and Behavioral Sciences

Publication Details
Guo, Y., Li, B., Zhang, J., Yuan, B., Xie, F. & Roberts, R. G. (2017). New ages for the Upper Palaeolithic site of Xibaimaying in the Nihewan Basin, northern China: implications for small-tool and microblade industries in north-east Asia during Marine Isotope Stages 2 and 3. Journal of Quaternary Science, 32 (4), 540-552.

Authors
Yujie Guo, Bo Li, Jia-Fu Zhang, Bao Yin Yuan, Fei Xie, and Richard G. Roberts

New ages for the Upper Palaeolithic site of Xibaimaying in the Nihewan Basin, northern China: implications for small-tool and microblade industries in northeast Asia during Marine Isotope Stages 2 and 3

Yu-Jie Guo[1]*, Bo Li[1], Jia-Fu Zhang[2], Bao-Yin Yuan[3], Fei Xie[4], Richard G. Roberts[1]

[1] *Centre for Archaeological Science, School of Earth and Environmental Sciences, University of Wollongong, Wollongong, NSW 2522, Australia*

[2] *MOE Laboratory for Earth Surface Processes, Department of Geography, College of Urban and Environmental Sciences, Peking University, Beijing 100871, China*

[3] *Institute of Geology and Geophysics, Chinese Academy of Sciences, Beijing 100029, China*

[4] *Cultural Relics of Hebei Province, Shijiazhuang 050000, China*

* *Corresponding author: yg991@uowmail.edu.au; yjguo87@gmail.com*

Abstract

It has been suggested that the ‘small tool’ and microblade Upper Palaeolithic industries coexisted in the Nihewan Basin of northern China for about 8–14 thousand years during Marine Isotope Stage (MIS) 2. This inference was based on uranium-series ages of around 15 and 18 ka for bovid teeth recovered from the ‘latest’ small-tool site of Xibaimaying—the youngest occurrence of such tools in the region—and optically stimulated luminescence (OSL) dating of the earliest typical microblade site (Youfang: ~26–29 ka). In this study, we re-dated the Xibaimaying site using single-grain OSL methods and the resulting ages indicate that the cultural layer was deposited 46 ± 3 ka ago, during MIS 3—more than 20 millennia earlier than previously thought and older also than the so-called earliest ‘primitive’ and typical microblade tools found at Zhiyu (~31–39 ka cal BP) and Youfang. These new ages for human occupation of Xibaimaying remove support for the parallel development of the small-tool and microblade industries in the Nihewan Basin during the Upper Palaeolithic, but reliable age estimates from additional sites are needed to confidently infer the nature of the chronological relationship between these two Upper Palaeolithic industries and the associated toolmakers.

Keywords: quartz OSL; single-grain dating; Chinese Palaeolithic; stone artefacts; MIS 3.

Introduction

The 'small tool' industry is one of the two major Palaeolithic traditions in North China (Jia et al., 1972). It was first recognised and classified as the Zhoukoudian Locality 1–Zhiyu series (in the boat-shaped scrapers–burins tradition) (Jia et al., 1972), and was later named the small-tool technology or industry (Zhang, 1990; Liu, 2014). The small-tool assemblage is characterised by rare prepared cores and production of small, irregular flakes, some of which were probably used as scrapers (Zhang, 1999). The small-tool industry is considered to be the most abundant Palaeolithic industry known from northern China during the Pleistocene (Zhang, 1999), found across northern China (107°29'–122°10' E, 34°10'–41°15' N) during the Lower and Middle Palaeolithic and across almost all of China (87°21'–126°18' E, 24°55'–45°36' N) in the Upper Palaeolithic (Fig. 1) (Zhang, 1999). Representative sites include Zhoukoudian Locality 1 (Teihard de Chardin and Pei, 1932), Zhoukoudian Locality 15 (Gai, 1991), Salawusu (Teihard de Chardin and Licent, 1924), Zhiyu (Jia et al., 1972) and Xiaonanhai (An, 1965) (Fig. 1).

The small-tool industry is commonly considered to have originated and developed primarily in the Nihewan Basin (Fig. 1) since the Early Pleistocene (Liu, 2014). The Basin is key to the study of the Palaeolithic archaeology of East Asia, with more than 100 Palaeolithic sites spanning the entire Pleistocene (e.g., Schick et al., 1991; Zhu et al., 2001, 2004; Hou, 2008; Norton and Gao, 2008; Nian et al., 2014; Guo et al., 2016). The small-tool industry is considered to be 'continuous' from the Early to the Late Pleistocene (Liu et al., 2013), whereas the typical microblade industry emerged ~29 ka ago in this region (Nian et al., 2014). Representative small-tool sites in the Basin include Heitugou (~1.77–1.95 Ma: Wei et al., 2016), Majuangou (~1.66 Ma: Zhu et al., 2004), Xiaochangliang (~1.36 Ma: Zhu et al., 2001), Donggutuo (~1.1 Ma: Wang et al., 2005), Sankeshu (~200–300 ka: Hou et al., 2010), Xujiayao (~240 ka: Tu et al., 2015, or ~220–160 ka: Mu et al., 2015 and Zhang et al., 2015), Banjingzi (~86 ka: Guo et al., 2016), Zhiyu (~31–36 ka cal BP: Institute of Archaeology of Chinese Academy of Social Sciences, 1991, or ~36–39 ka cal BP: Yuan, 1993; and discussed further below) and Xibaimaying (~15–18 ka: Xie and Yu, 1989). These form an 'evolutionary line' for the small-tool industry during the Pleistocene (Liu, 2014).

Although the small-tool industry appears to have developed gradually in the Nihewan Basin over the last two million years, some 'advanced' or 'developed' traits have been reported at several sites, including Donggutuo, Xujiayao, Banjingzi and Zhiyu (Liu et al., 2013; Liu, 2014). One of the most important discoveries associated with small-tool lithic assemblages is the prepared, wedge-shaped core found at Donggutuo (the so-called 'Donggutuo Core': Hou et al., 1999; Hou, 2003, 2008). Some archaeologists consider the 'Donggutuo Core', which was used to produce small elongated flakes, as the ancestral form of the wedge-shaped, microblade cores found at Upper Palaeolithic sites across northeast Asia (Hou et al., 1999; Hou, 2003, 2008). Donggutuo Cores (or their equivalent) have also been described from the sites of Sankeshu, Xujiayao and Zhiyu in the Nihewan Basin, Zhoukoudian Localities 1 and 15 and Shuidonggou in northern China (Liu et al., 2013), Kara-Bom, Denisova and Ust-Karakol in southern Siberia (Hou, 2005), and Chikhen Agui Cave in Mongolia (Derevianko, 2001).

During the Upper Palaeolithic, lithic technologies in the Nihewan Basin became more complex. It has been argued that the microblade culture and the small tool culture "developed simultaneously, but without mutual influence" (Liu et al., 2013). Animal bone fragments from the Zhiyu site have been dated by ^{14}C to 28,945 ± 1370

BP (Institute of Archaeology of Chinese Academy of Social Sciences, 1991) and 33,155 ± 645 BP (Yuan, 1993), which correspond to calendar-year ages (95% confidence intervals) of 30.5–35.7 and 35.8–38.8 ka cal BP, respectively. The lithic technology at this site has been described as 'transitional' between small-tool and microblade (Jia et al., 1972; Jia, 1978) or 'primitive' microblade (Chun, 1984). According to some other archaeologists, the stone artefacts at this site may not be related to microblade technology, but their alternative interpretations have yet to be published. The Youfang site—dated to about 26–29 ka based on OSL analyses of quartz grains (Nian et al., 2014)—is considered to be the earliest 'typical' microblade site known from the northern high latitudes of China (40°N) (Nian et al., 2014), while the Xibaimaying site is considered to be the 'latest' small-tool site discovered in the Nihewan Basin (Xie et al., 2006). The age range of ~15–18 ka for Xibaimaying is based on uranium-series dating of bovid teeth (Xie and Yu, 1989). These ages, together with those for Zhiyu and Youfang, have led to the suggestion that the small-tool and microblade industries coexisted in the Nihewan Basin (Xie et al., 2006; Liu et al., 2013; Jia et al., 2015) from at least ~30 ka ago until as recently as ~15 ka ago.

The coexistence of these two industries raises a number of questions, including the reason for the lack of technological 'development' at Xibaimaying, the youngest of these sites. Jia et al. (2015) showed that the availability of raw material was not the main factor governing the absence of microblade technology at this site. They also argued that microblade technology did not appear to spread as an adaptive response to deteriorating environmental conditions associated with the Last Glacial Maximum (LGM), ~21 ka ago, as has been hypothesised previously (Institute of Archaeology of Northern Ethnicity and Department of Archaeology and Museology, Renmin University, 2006). Others have proposed that microblade technology was introduced to northern China by people migrating from Siberia or Mongolia (e.g., Keates, 2007; Kuzmin, 2007; Nian et al., 2014), whereas Xibaimaying might be inhabited by a local group who maintained their small-tool tradition (Jia et al., 2015). If so, then the prehistory of the Nihewan Basin might be much complex than currently thought (Liu et al., 2013).

These archaeological discussions are based on the presumption that the ages for Xibaimaying and Youfang are accurate, which may not be true. In particular, uranium-series dating is now well-known to be poorly suited to faunal remains, owing to their open-system geochemical behaviour (Hellstrom and Pickering, 2015). Uranium-series dating typically provides only minimum age estimates for fossil bones and teeth, even when modern methods of data collection and analysis are used (Grün et al., 2014). In view of the questionable accuracy of the uranium-series ages for Xibaimaying, the aim of this study is to provide more reliable estimates of age for human occupation of this 'latest' small-tool site using OSL dating methods applied to quartz grains. This method has previously been applied to deposits elsewhere in the Nihewan Basin (e.g., Zhao et al., 2010; Nian et al., 2014; Guo et al., 2015, 2016), so OSL dating of Xibaimaying would enable a direct chronological comparison with other sites in the region—including the microblade site of Youfang.

The study site

The Xibaimaying site (40°07'28"N, 114°14'19"E, 915 m above mean sea level) is located on the second terrace of the east bank of the Nangou gully (Fig. 2a), a tributary of the Sanggan River, ~300 m south of Xibaimaying village in Yangyuan County of Hebei Province (Xie et al., 2006). The site was discovered in 1985 and a total area of 76 m^2 excavated in 1985 and 1986. The sedimentary profile of the east wall of the excavation pit consists of 5 layers (Fig. 2b,d), which are as follows (top to bottom): soil (~0.1 m in depth), red-yellow silty clay (~0.7 m), white-yellow silty clay (~0.5 m), yellow silty clay (~1.4 m) and fluvially interbedded grey-green and red-yellow clayey fine sands (~0.4 m). The basal unit (Layer 5) yielded abundant stone artefacts, animal bone remains (Fig. 2c), burnt soil blocks, burnt bones and charcoal, and represents the cultural layer at this site (Xie and Yu, 1989).

A total of 1546 stone artefacts have been recovered from the cultural layer at this site (Xie and Yu, 1989), including cores (n = 78), flakes (n = 184), tools (n = 230) and waste objects (e.g., chunks, debris; n = 1054) produced during the process of lithic reduction. Some typical stone artefacts are shown in Fig. 3. The general properties of the stone artefacts are described by Xie and Yu (1989) in Chinese, so we have summarised them below in English:

(1) Cores include 75 hammered cores and 3 percussion cores. Most of the hammered cores are small, with the largest and smallest being 104×74×52 mm and 18×10×9 mm in size, respectively. The hammered cores can be further divided into single platform (n = 31), double platform (n = 27) and multi-platform (n = 17). Platforms are dominated by plain platforms, followed by natural platforms; scarred platforms are rare. Some multi-platform cores are nearly spheroidal in shape. Several single-platform cores (Fig. 3i,j) show some traits of micro-cores: cone-shaped with plain platforms and flaking scars that are elongated and dense. The three percussion cores are small in size (< 30 mm) and slightly elongated in shape (Fig. 3k,l).

(2) Flakes are composed of hammered flakes (n = 179) and percussion flakes (n = 5). The flake platforms are dominated by plain platforms, followed by natural

platforms and scarred platforms; prepared platforms are rare. Flakes are generally irregular in shape, but dominated by flakes that are wider than they are long. Most of the flakes are small in size, with the largest and smallest being 92×98×25 mm and 8×12×3 mm, respectively.

(3) Tools are commonly less than 40 mm in maximum dimension, dominated by scrapers (n = 216) associated with points (n = 11), burins (n = 2) and a chopper (n = 1). The tool blanks are mainly flakes (66%) and chunks (34%). The fracture method was mainly hammering. Most of the tools are retouched, with fine regular scars, and several scrapers have been retouched by indirect pressure.

(4) Raw materials are dominated by pyroclastic rock (35.6%) associated with vein quartz (18.6%), agate (13.6%), siliceous limestone (12.7%), flint (9.9%), hornstone (6.1%), quartz sandstone (2.1%) and schist (1.4%). The tools, however, are mostly made from flint and agate. Du (2003) analysed the raw materials at Xibaimaying and argued that the agate, flint and vein quartz are similar as those at the Shenquansi site (Fig. 1), the pyroclastic rocks are similar to those at the Xinmiaozhuang site (Fig. 1) and the occupants of Xibaimaying had no preference for a particular raw material type; all the raw materials are available within ~10 km of the site (Du, 2003).

The cultural layer contains abundant vertebrate and freshwater mollusc fossils (Xie and Yu, 1989). The identified freshwater molluscs include *Corbicula fluminea*, *Gyraulus convediusculus*, *G. compressus* and *Radxi auricularia*. The identified vertebrate fossils include *Strothio* sp. (ostrich), *Bos primigenius* (cow), *Equus pnzewalskyi* (horse), *E. hemionus* (donkey), *Gazella przewalskyi* (antelope), *Cervus* sp. (deer), *Sus* sp. (pig), *Coelodonta* sp. (rhinoceros), *Elephas* sp (elephant) and

Carnivora (not identifiable to genus or species). A total of 315 fossil bones, most of which are broken, were analysed by Xie and Yu (1989); 24 bones had been gnawed by rodents and 31 were identified as bone tools (e.g., Fig. 3m). The artefacts from this site are thought to be in primary depositional context, based on the well-preserved state of the cultural remains and the lack of evidence of any disturbance of the artefact-bearing layer (Xie et al., 2006). This site was probably used to manufacture stone tools, with the lithic reduction process accounting for the large number of waste objects recovered (Xie et al., 2006). Two uranium-series ages of 18 ± 1 and 15 ± 1 ka were obtained for bovid teeth from the cultural layer (Xie and Yu, 1989), on which basis the site was assigned to the Upper Palaeolithic.

In this study, five sediment samples (XBMY-OSL-1 to -5) were collected from the sedimentary profile at Xibaimaying (Fig. 2). Only four of these samples were subsequently prepared for OSL dating (XBMY-OSL-1, -2, -3 and -5), of which XBMY-OSL-1 was collected from the cultural layer (Layer 5).

OSL dating

Over the last 30 years, OSL dating has been become one of the most widely used numerical dating methods to determine burial ages for Quaternary sediments in variety of a depositional environments (Huntley et al., 1985; Aitken, 1998; Lian and Roberts, 2006; Jacobs and Roberts, 2007; Preusser, 2008; Rhodes, 2011; Wintle, 2014; Roberts et al., 2015). The method determines the time elapsed since common minerals, such as quartz and potassium feldspar (K-feldspar), were last exposed to light or heat (temperatures above ~300 °C). Exposure to sunlight empties the light-sensitive electron ‘traps’ in these minerals, and these traps then steadily refill with electrons while the mineral grains are buried in the ground, where they are shielded from sunlight and exposed to background levels of ionising radiation. In the laboratory, the grains are exposed to green or blue light, which causes the light-sensitive electrons to escape from their traps and their subsequent recombination at luminescence centres results in the emission of photons (i.e., OSL).

The burial time of a mineral grain can be estimated from the intensity of this OSL signal, by converting it into a dose equivalent (D_e) and dividing the D_e by the environmental dose rate. The latter represents the rate of supply of ionising radiation to the grain over the period of burial from environmental sources of alpha, beta and gamma radiation (due to the decay of radionuclides in the uranium and thorium decay chains and ^{40}K) and from cosmic rays.

Sample collection, preparation and dose rate determination

Block samples about 10x10x10 cm in size were collected from the cleaned section faces. After the blocks were removed, they were immediately wrapped in light-proof plastic and transported to the Luminescence Dating Laboratory at the University of Wollongong for preparation and analysis. In the laboratory, the outer layer (~2 cm) of the blocks was removed under subdued red light and the materials from the outer layer were used for dose rate determination. Quartz grains were extracted from each of the trimmed blocks using standard mineral separation procedures (Aitken, 1998). Carbonate and organic matter were removed using HCl and H_2O_2 solutions, respectively, and quartz grains of 125–150 μm in diameter were isolated by wet sieving and density separation (2.62 and 2.70 g/cm^3). These grains were then etched in 40% HF acid for 40 min to dissolve any remaining feldspar grains and to remove the alpha-irradiated outer layer of each quartz grain. The etched quartz grains were then washed in HCl solution to remove any precipitated fluorides.

For dose rate determinations, the beta dose rates were measured directly using a low-level beta counter (Bøtter-Jensen and Mejdahl, 1988; Jacobs and Roberts, 2015) and the gamma dose rates were calculated from the U and Th contents determined by thick-source alpha counting (Aitken, 1985) and the K contents measured by X-ray fluorescence spectroscopy. Cosmic-ray dose rates were estimated from the burial depth of each sample and the latitude, longitude and altitude of Xibaimaying (Prescott and Hutton, 1994). As the sampled section at this site has been aerially exposed for a prolonged period since excavation, it is likely to have dried out considerably. Accordingly, we did not adjust the dry beta, gamma and cosmic-ray dose rate using the measured (field) water contents, but instead used water contents of 15 ± 5% for fluvial sample XBMY-OSL-1 and 10 ± 3% for samples XBMY-OSL-2, 3 and 5 (probably aeolian or waterlain aeolian deposits), following Guo et al. (2016). The calculated OSL ages increase (or decrease) by ~1% for each 1% increase (or decrease) in water content. A small, internal dose rate of 0.03 ± 0.01 Gy/ka due to U and Th inclusions within the quartz grains (e.g., Jacobs et al., 2008) was included in the total environmental dose rate for each of the four samples.

D_e determination

OSL measurements were made on individual grains using standard single-grain discs drilled with 100 holes, each 300 μm wide and 300 μm deep (Bøtter-Jensen et al., 2000). Discs were checked under the microscope to verify that each hole contained only one grain; this was true for most holes, but some contained two or three grains. For the latter holes, the OSL signals should be derived predominantly from only one grain, because ~90% of the total light sum for our samples originates from the ~11% brightest grains (Figure S1). Thus, the OSL results for our samples are considered representative of true single-grain analyses. Measurements were performed on an automated Risø TL/OSL-DA-20 reader equipped with a calibrated $^{90}Sr/^{90}Y$ beta source, a green (532 nm) laser for optical stimulation of individual grains and blue light-emitting diodes (470 ± 30 nm) to stimulate single aliquots in the preheat temperature test described below. The ultraviolet OSL emissions were detected by an Electron Tubes Ltd 9235B photomultiplier fitted with Hoya U-340 filters.

D_e measurements were made using the single-aliquot regenerative-dose (SAR) procedure (Murray and Roberts, 1998; Roberts et al., 1998a, 1998b; Galbraith et al., 1999; Murray and Wintle, 2000, 2003; Wintle and Murray, 2006; Jacobs et al., 2006, 2008). In this procedure, the dose response curve (DRC) for each grain is constructed using the sensitivity-corrected OSL signals (L_x/T_x) induced from a series of regenerative doses, including a duplicate dose and a zero dose to monitor the recycling ratio and the extent of recuperation, respectively. The D_e value of each grain was obtained by interpolating the sensitivity-corrected natural OSL signal (L_n/T_n) on to its corresponding DRC, which was fitted using a single saturating exponential function, an exponential plus linear function, or the sum of two saturating exponential functions—whichever provided the best fit to the L_x/T_x data. For each D_e estimate, the associated uncertainty includes photon counting statistics, an instrumental irreproducibility error of 2% for each OSL measurement (following Jacobs et al., 2006), the curve fitting error, and the error involved in determining the calibrated beta dose rate delivered to each grain position on a disc.

We also included an additional regenerative dose cycle at the end of the SAR sequence (using an infrared stimulation for 40 s at 50 °C prior to measuring the OSL signal) to determine the OSL IR depletion ratios and check for any remnant feldspar contamination (Duller, 2003). Table S1b lists the full SAR measurement sequence used for single grains in this study. The net OSL signals used for D_e estimation were calculated as the sum of counts in the first 0.12 s of OSL decay minus a 'late light' background estimated from the mean count rate over the final 0.12 s. Grains were held for 0.1 s before and after optical stimulation to monitor and minimise any interference from isothermal decay. A typical OSL decay curve and DRC is shown in Fig. 4 for a single grain of quartz from sample XBMY-OSL-1.

To choose a suitable preheat temperature, we made D_e measurements on single aliquots of sample XBMY-OSL-5 (where each aliquot consisted of ~200 grains) using the SAR procedure listed in Table S1a and preheat temperatures of between 180 and 300 °C (step 2). Thirteen to twenty aliquots were measured at each preheat temperature. The net OSL signal was determined as the sum of counts in the first 0.64 s of OSL decay minus a background estimated from the mean count rate over the final 3.2 s. The preheat given in step 5 after a fixed test dose (12.6 Gy) was set 40 °C lower than that applied to the natural and regenerative doses; the sole exception was the 180 °C preheat in step 2, which was accompanied by a preheat of 160 °C in step 5. At the end of each SAR cycle, a 'hot optical bleach' was performed at a temperature 20 °C higher than the corresponding preheat in step 2, to erase any remnant OSL signal. The weighted mean D_e values and the recycling and recuperation ratios are plotted as a function of preheat temperature in Fig. 5. This plot shows that a D_e 'plateau' (46 ± 3 Gy) is obtained at preheat temperatures of 220–260 °C and that the recycling ratios are consistent with unity at all preheat temperatures (except 280 °C). This experiment indicates, therefore, that preheat temperatures of between 220 and 260 °C should be suitable for determining D_e values for the Xibaimaying samples.

A dose recovery test (Galbraith et al., 1999) was conducted using single grains of quartz from sample XBMY-OSL-1. Measurement conditions included a natural and regenerative dose preheat of 240 °C and a test dose preheat of 200 °C, based on the preheat plateau test mentioned above. Two thousand grains were first bleached for ~2 hr using a Dr Hönle solar simulator (Model: UVACUBE 400) and a dose of 140 Gy was then given to the bleached grains as the surrogate 'natural' dose. The grains were measured using the procedures listed in Table S1b, with the test dose fixed at 30 Gy. Grains were rejected if the resulting OSL data failed to satisfy a series of well-established criteria similar to those proposed by Jacobs et al. (2006), namely if: 1) the initial T_n signal was less than 3 times its corresponding background or its relative error was greater than 25%; 2) the recuperation ratio was larger than 10%; 3) the recycling ratio or OSL IR depletion ratio differed from unity by more than 2σ; 4) the DRC provided an obviously poor fit to the L_x/T_x data points; and 5) the L_n/T_n value was consistent with or exceeded the saturation level of the corresponding DRC. The number of grains rejected according to each of these criteria are summarised (in order of rejection) in Table S2.

A total of 122 grains (6% of the 2000 grains measured) were accepted for dose determination after applying these rejection criteria. The distribution of the dose recovery ratios (i.e., ratios of measured to given dose) for all accepted grains is shown in Fig. 6a. The over-dispersion (OD) value for this dose distribution, calculated using the Central Age Model (CAM: Galbraith et al., 1999; Galbraith and Roberts, 2012) is 23.5 ± 2.9 % and the weighted mean ratio is 0.90 ± 0.03 (also calculated using the CAM). The latter value is slightly less than unity and indicates that the given dose was not recovered fully using the measurement conditions and/or the data selection criteria.

Li et al. (2016) have suggested that if a significant proportion of grains in a sample yield infinite D_e values (i.e., L_n/T_n values in the saturated region of the DRC), then this could result in a truncated D_e distribution and a corresponding underestimation of true D_e and age. They suggested that a more reliable estimate of D_e could be obtained based on those grains that saturate at larger doses. Rejection of quartz grains with low characteristic saturation doses (D_0 values) has been used previously in single-grain OSL dating to improve the accuracy of the resulting D_e estimates (e.g., Duller, 2012; Gliganic et al., 2012). We hypothesised, therefore, that underestimation of the applied dose in the dose recovery test may be due to the given dose (140 Gy) lying at or close to the saturation level of a significant proportion of the measured grains.

To test this hypothesis, after applying the first 4 rejection criteria mentioned above, we sorted the accepted grains according to their D_0 values, which we calculated from the DRCs fitted to the L_x/T_x data points using a single saturating exponential function; the latter has the form $I = I_0(1 - e^{-D/D_0}) + c$, where I is the sensitivity-corrected OSL intensity, D is the regenerative dose, and I_0 and c are constants. We then applied the fifth rejection criterion to recalculate the recovered dose (using the CAM) while increasing the minimum D_0 threshold from 0 to 300 Gy in steps of 30 Gy. The CAM dose estimates, OD values and the numbers of accepted and saturated grains at different minimum D_0 thresholds are summarised in Table S3, and the corresponding dose recovery ratios are plotted in Fig. 6b. The dose recovery ratios increase in concert with the D_0 threshold, achieving values consistent with unity at a D_0 threshold of 90 Gy and above.

We then scrutinised these data further to identify the D_0 threshold at which the number of the saturated grains reached zero (Table S3); we define this value as the 'optimum-D_0 threshold'. For the dose recovery test, the optimum-D_0 threshold is 120 Gy—resulting in a dose recovery ratio of 0.97 ± 0.04 (Fig. 6b), which is consistent with unity (Table S3). For the single-grain measurements of the older samples from Xibaimaying, therefore, it would appear necessary to first sort the accepted grains according to their grain-specific D_0 values and then determine the optimum-D_0 threshold to avoid truncating the upper end of the single-grain D_e distribution.

The preheat temperature test on sample XBMY-OSL-5 and the dose recovery test and D_0-threshold procedure applied to sample XBMY-OSL-1 have yielded a set of SAR measurement conditions and data analysis procedures that should be suitable for dating the Xibaimaying samples. We measured a total of 3400, 2800, 1400 and 1900 grains of samples XBMY-OSL-1, -2, -3 and -5, respectively, using the procedures in Table S1b; the test dose was fixed at 30 Gy for samples XBMY-OSL-1, -2 and -3 and 10 Gy for sample XBMY-OSL-5. Of the measured grains, 135, 141, 71 and 82 were accepted for samples XBMY-OSL-1, -2, -3 and -5, respectively, after applying the 5 rejection criteria described above (Table S2). The D_e values for these grains are displayed in Fig. 7. Note that these D_e estimates were obtained before applying the optimum-D_0 threshold criterion, so that we could evaluate its subsequent effect on the D_e distributions.

Samples XBMY-OSL-1, -2, -3 and -5 each contained some saturated grains, amounting to approximately 29, 29, 13 and 3% of the total number of accepted grains, respectively (Table S2). The CAM D_e values of samples XBMY-OSL-1 and -2, in particular, are thus potentially underestimated, owing to the high proportion (>20%) of saturated grains. After applying the first 4 rejection criteria mentioned above, we then sorted the accepted grains by the D_0 values of their DRCs. The corresponding recalculated CAM D_e values are plotted as a function of D_0 threshold in Fig. 8; the optimum-D_0 threshold values are 120, 150, 120 and 30 Gy for samples XBMY-OSL-1, -2, -3 and -5, respectively (Table S3). For samples XBMY-OSL-1 and -2, the CAM D_e estimates attain a 'plateau' close to and above the optimum-D_0 threshold value (zero saturated grains), while the CAM D_e values are statistically consistent for all D_0 thresholds for samples XBMY-OSL-3 and -5 due to less saturated grains (< 13 %) in the latter two samples. The D_e estimates for grains with D_0 values at or above the optimum thresholds are displayed as solid triangles in Fig. 7. The OD values for these samples are reduced from 46–50% to 35–42% after applying the optimum-D_0 threshold criterion, and the D_e values appear to be randomly distributed around a central value. We calculated the final D_e estimates using the CAM, which yielded values of 147.2 ± 7.5, 112.4 ± 6.5, 82.7 ± 7.5 and 39.3 ± 2.5 Gy for samples XBMY-OSL-1, -2, -3 and -5, respectively. We note that the single-grain D_e value for sample XBMY-OSL-1 (39.3 ± 2.5 Gy) is consistent at 2σ with its single-aliquot D_e 'plateau' value (46 ± 3 Gy).

Ages and implications

Table 1 summarises the dose rates, D_e values and OSL ages for the four samples from Xibaimaying. The ages are in correct stratigraphic order (Fig. 2d), increasing down-profile from early Holocene in Layer 2 (13 ± 1 ka: XBMY-OSL-5) to early MIS 2 or late MIS 3 in the middle and lower parts of Layer 4 (24 ± 2 and 32 ± 2 ka: XBMY-OSL-3 and -2, respectively), with the basal, artefact-bearing sediments (Layer 5) deposited in mid-MIS 3 (46 ± 3 ka: XBMY-OSL-1). The latter age is consistent with a recent ^{14}C age determination of 47–50 ka cal BP for a fragment of ostrich eggshell recovered from the cultural layer at this site (Ying Guan, Institute of Vertebrate Paleontology and Paleoanthropology, personal communication). The coherent stratigraphic ordering of OSL ages, and the agreement with the ^{14}C age determination for the cultural layer, supports the reliability of our chronology. These results also suggest that the uranium-series ages of 18 ± 1 and 15 ± 1 ka obtained from bovid teeth (Xie and Yu, 1989) should be viewed as minimum estimates of age, as might be expected for such materials given their open-system geochemical behaviour (Grün et al., 2014).

The age of 46 ± 3 ka for the cultural layer potentially falls within the 43–51 ka period of MIS 3 during which the local landscape was indicated covered by sparse desert-steppe vegetation in lowland areas and the northern Loess Plateau, merging into a mixture of steppe and coniferous forest in the surrounding highlands (Liu et al., 2014). The pollen and spore composition has also been examined for the cultural layer at the site, and this also indicates a sparse coniferous forest and desert steppe vegetation (Xie and Yu, 1989): herbs (mainly Artenmisia) account for 93.4% of the pollen and spores, with trees (mostly Pinus and Picea) and ferns accounting for only 4.4% and 2.2%, respectively.

As mentioned above, it has long been regarded by Chinese archaeologists that the small-tool and microblade industries coexisted without mutual influence in the Nihewan Basin, based largely on the uranium-series ages for Xibaimaying (Xie and Yu, 1989; Xie et al., 2006; Liu et al., 2013; Jia et al., 2015). Our OSL chronology for this site shows that the small-tool artefacts are 14–25 ka older than the microblade artefacts found at the Youfang site (26–29 ka), which are the earliest known occurrence of typical microblade tools in the Nihewan Basin. The ages of the artefacts at Xibaimaying are also older than those at the Zhiyu site (~31–39 ka cal BP), which are considered by some archaeologists (e.g., Jia et al., 1972; Jia, 1978) to exhibit 'transitional' traits between small-tool and microblade technologies. The new ages reported here, therefore, are compatible with a developmental trend in stone tool technology in the Nihewan Basin from mid-MIS 3 to early MIS 2, from small-tool technology (Xibaimaying) to ‘transitional’ small-tool/microblade artefacts (Zhiyu) to typical microblade technology (Youfang). Fig. 9 provides a graphical summary of the existing and new chronologies for the different technologies in the basin.

The origin of the microblade technology in North China has been the subject of considerable debate over the past few decades, as summarised in the reviews by Zhu (2006: 130–135) and Yi et al. (2016). There are two general hypotheses: this technology emerged in situ from the local small-tool tradition (e.g., Jia et al., 1972; Jia, 1978) or was introduced from northern Siberia or Mongolia (e.g., Keates, 2007; Kuzmin, 2007). The first hypothesis is based on discoveries of ‘microblade traits’ at some local small-tool sites (e.g., the ‘Donggutuo Core’); whereas the second hypothesis argued that the microblades were not “simply a type of small tool”, but “stand for products of a special technology including microblades, microblade cores, and tools made with microblades”, and this hypothesis has received support from the chronological sequence of microblade sites in Siberia, Mongolia and North China (Yi et al., 2016: 131). Microblade artefacts appear in Siberia as early as ~35 ka (Derevianko et al., 1998) and the earliest known sites in China with typical microblade artefacts are Longwangchan and Youfang (Fig. 1), which have been dated by OSL to 25–29 ka (Zhang et al., 2011) and 26–29 ka (Nian et al., 2014), respectively.

Our OSL dating results for Xibaimaying are consistent with the small-tool industry preceding the microblade industry in the Nihewan Basin and, thus, lend support to the ‘local origin’ hypothesis for microblade technology. But in the absence of independent evidence for the identity of the toolmakers, we cannot discount the possibility that the technology was introduced by people migrating from northern Siberia or Mongolia. Furthermore, an issue with the study of the origins of the microblade in North China is that many Chinese archaeologists have focussed on artefacts found in northeast Asia. Microblade tools have been reported from earlier contexts in other parts of the world, such as ~71 ka in South Africa (Brown et al., 2012) and ~48 ka in India (Mishra et al., 2013; Basak et al., 2014), so a southern origin for this technology should also be taken into consideration. The key to revealing the origin of the microblade in North China will be to establish reliable spatial and temporal distribution patterns for this technology not only in northeast Asia but also throughout East and South Asia.

Conclusions

In this study, we have re-dated the 'latest' small-tool industry site (Xibaimaying) in the Nihewan Basin using single-grain OSL methods for quartz. Our chronology indicates that the cultural layer was deposited 46 ± 3 ka ago, corresponding to the middle of MIS 3, rather than the later part of MIS 2 as suggested previously by uranium-series dating of bovid teeth (Xie and Yu, 1989). A developmental trend in artefact technology is one inference from our data—that is, a change from the small-tool industry at Xibaimaying (46 ± 3 ka) to the earliest microblade at Zhiyu (31–39 ka cal BP) and the typical microblade at Youfang (26–29 ka). This pattern contrasts with the parallel development of these two lithic technologies in the basin during the Upper Palaeolithic (Fig. 9), which is the prevailing view among many archaeologists. However, until further archaeological and chronological studies are conducted on Late Pleistocene sites containing small-tool and microblade artefacts in northern China—and in other parts of Asia—we cannot be certain of the temporal relation between these two industries or the geographic origin of the local microblade technology.

Acknowledgements

This study was supported by postgraduate scholarships from the China Scholarship Council and the University of Wollongong to Y.G. (201206010053), an Australian Research Council Future Fellowship to B.L. (FT140100384), a grant from the National Natural Science Foundation of China to J.Z. (NSFC, No. 41471003), and an Australian Research Council Australian Laureate Fellowship to R.G.R. (FL130100116). We thank Weiwen Huang, Yue Hu, Yongmin Meng, Qi Wei, Shengquan Cheng, Fagang Wang, Yang Liu and others who helped with the field investigations and collection of OSL samples and relevant literature.

Supporting Information

Additional supporting information is available in the online version of this article.

Figure S1. The single-grain 'brightness' distribution for 200 individual grains of sample XBMY-OSL-1. The cumulative light sum of the L_n signals (shown on the *y*-axis) is plotted as a function of the corresponding proportion of grains (shown on the *x*-axis).

Table S1. Single-aliquot regenerative-dose (SAR) procedures used in this study.

Table S2. Numbers of single grains measured, rejected and accepted for D_e determination.

Table S3. Numbers of accepted and saturated grains at various D_0 thresholds, and corresponding CAM and OD values.

References

Aitken MJ. 1985. *Thermoluminescence Dating*. Academic Press: London.

Aitken MJ. 1998. *An Introduction to Optical Dating*. Oxford University Press: Oxford.

An ZM. 1965. Trial excavation of the Paleolithic cave of Hsiao-nan-hai in Anyang, Honan (in Chinese). *Acta Archaeologica Sinica* 1: 1–26.

Basak B, Srivastava P, Dasgupta S, Kumar A, Rajaguru SN. 2014. Earliest dates and implications of microlithic industries of Late Pleistocene from Mahadebbera and Kana, Purulia district, West Bengal. *Current Science* 107: 1167–1171.

Bøtter-Jensen L, Bulur E, Duller GAT, Murray AS. 2000. Advances in luminescence instrument systems. *Radiation Measurements* 32: 523–528.

Bøtter-Jensen L, Mejdahl V. 1988. Assessment of beta dose rate using a GM multicounter system. *Nuclear Tracks and Radiation Measurements* 14: 187–191.

Brown KS, Marean CW, Jacobs Z, Schoville BJ, Oestmo S, Fisher EC, Bernatchez J, Karkanas P, Matthews T. 2012. An early and enduring advanced technology originating 71,000 years ago in South Africa. *Nature* 491: 590–593.

Chen, C. 1984. The microlithic in China. *Journal of Anthropological Archaeology* 3: 79–115.

Derevianko AP. 2001. The Middle to Upper Palaeolithic transition in the Altai (Mongolia and Siberia). *Archaeology, Ethnology and Anthropology of Eurasia* 3: 70–103.

Derevianko AP, Agadzhanian AK, Baryshnikov GF, Dergacheva MI, Dupal TA, Malaeva EM, Markin SV, Molodin VI, Nikolaev SV, Orlova LA, Petrin VT, Postnov

AV, Ul'ianov VA, Fedeneva IN, Foronova IV, Shun'kov MV. 1998. *Arkheologiya, geologiya i paleogeografiya pleistozena i golozena Gornogo Altaya (Archaeology, Geology, and Paleogeography of the Pleistocene and Holocene of the Mountainous Altai)* (in Russian). Institute of Archaeology and Ethnography Press: Novosibirsk.

Duller GAT. 2003. Distinguishing quartz and feldspar in single grain luminescence measurements. *Radiation Measurements* 37: 161–165.

Duller GAT. 2012. Improving the accuracy and precision of equivalent doses determined using the optically stimulated luminescence signal from single grains of quartz. *Radiation Measurements* 47: 770–777.

Du SS. 2003. A preliminary study on raw material exploitation in Middle–Upper Palaeolithic sites in Nihewan Basin (in Chinese with English abstract). *Acta Anthropologica Sinica* 22: 121–130.

Gai P. 1991. Microblade tradition around the northern Pacific rim: a Chinese Perspective. In *Proceedings of the XIII International Quaternary Conference*, Institute of Vertebrate Palaeontology and Palaeoanthropology (ed). Scientific and Technological Publishing House: Beijing; 21–31.

Galbraith RF, Roberts RG, Laslett GM, Yoshida H, Olley JM. 1999. Optical dating of single and multiple grains of quartz from Jinmium rock shelter, northern Australia: Part I, experimental design and statistical models. *Archaeometry* 41: 339–364.

Galbraith RF, Roberts RG. 2012. Statistical aspects of equivalent dose and error calculation and display in OSL dating: an overview and some recommendations. *Quaternary Geochronology* 11: 1–27.

Gligani LA, Jacobs Z, Roberts RG. 2012. Luminescence characteristics and dose distributions for quartz and feldspar grains from Mumba rockshelter, Tanzania. *Archaeological and Anthropological Sciences* 4: 115–135.

Grün R, Eggins S, Kinsley L, Moseley H, Sambridge M. 2014. Laser ablation U-series analysis of fossil bones and teeth. *Palaeogeography, Palaeoclimatology, Palaeoecology* 416: 150–167.

Guo YJ, Li B, Zhang JF, Roberts RG. 2015. Luminescence-based chronologies for Palaeolithic sites in the Nihewan Basin, northern China: First tests using newly developed optical dating procedures for potassium feldspar grains. *Journal of Archaeological Science: Reports* 3: 31–40.

Guo YJ, Li B, Zhang JF, Yuan BY, Xie F, Roberts, RG. 2016. Luminescence ages for three 'Middle Palaeolithic' sites in the Nihewan Basin, northern China, and their archaeological and palaeoenvironmental implications. *Quaternary Research* 85: 456–470.

Han F, Bahain JJ, Boëda É, Hou Y, Huang W, Falguères C, Rasse M, Wei G, Garcia T, Shao Q, Yin G. 2012. Preliminary results of combined ESR/U-series dating of fossil teeth from Longgupo cave, China. *Quaternary Geochronology* 10: 436–442.

Hellstrom J, Pickering R. 2015. Recent advances and future prospects of the U–Th and U–Pb chronometers applicable to archaeology. *Journal of Archaeological Science* 56: 32–40.

Hou YM. 2008. The "Donggutuo core" from Donggutuo industry of Lower Pleistocene in the Nihewan Basin, North China and its indication. *L'Anthropologie* 112: 457–471.

Hou YM, Liu Y, Li YH, Liu H. 2010. A report on the 2008 test excavation at the Sankeshu Paleolithic site in the Nihewan Basin (in Chinese with English abstract). *Acta Anthropologica Sinica* 29: 227–241.

Hou YM, Wei Q, Feng XW, Lin SL. 1999. Re-excavation at Donggutuo in the Nihewan Basin, North China (in Chinese with English abstract). *Quaternary Sciences* 2: 139–147.

Hou YM. 2003. Naming and preliminary study on the category of the “Donggutuo core” (in Chinese with English abstract). *Acta Anthropologica Sinica* 22: 279–292.

Hou YM. 2005. Shuidonggou: A vane of intercommunication between the East and the West? —Discussion about Small Tool Culture in North China and hypothesis of the “Lithic Road” (in Chinese with English abstract). *Quaternary Sciences* 25: 750–761.

Huang WW. 1964. On a collection of Paleoliths from Sanmen area in western Honan (in Chinese with English abstract). *Vertebrate PalAsiatica* 8: 162–177.

Huntley DJ, Godfrey-Smith DI, Thewalt MLW. 1985. Optical dating of sediments. *Nature* 313: 105–107.

Institute of Archaeology of Chinese Academy of Social Sciences. 1991. Radiocarbon dates in Chinese Archaeology (1965–1991) (in Chinese). Kaoguxuezhuankan 28. Culture Relic Press: Beijing.

Institute of Archaeology of Northern Ethnicity and Department of Archaeology and Museology, Renmin University. 2006. *The Archaeology of Northern Ethnicity* (in Chinese). Science Press: Beijing.

Jacobs Z, Roberts RG. 2007. Advances in optically stimulated luminescence dating of individual grains of quartz from archeological deposits. *Evolutionary Anthropology* 16: 210–223.

Jacobs Z, Roberts RG. 2015. An improved single grain OSL chronology for the sedimentary deposits from Diepkloof Rockshelter, Western Cape, South Africa. *Journal of Archaeological Science* 63: 175–192.

Jacobs Z, Duller GA, Wintle AG. 2006. Interpretation of single grain D_e distributions and calculation of D_e. *Radiation Measurements* 41: 264–277.

Jacobs Z, Wintle AG, Duller GAT, Roberts RG, Wadley L. 2008. New ages for the post-Howiesons Poort, late and final Middle Stone Age at Sibudu, South Africa. *Journal of Archaeological Science* 35: 1790–1807.

Jia LP, Gai P, You YZ. 1972. Report on the excavation at Zhiyu Paleolithic site in Shanxi Province (in Chinese). *Kaoguxuebao* 1: 39–58.

Jia LP, Wei T, Wang J. 1961. The Palaeolithic site of Kehe in Ruicheng, Shanxi province (in Chinese). *Archaeology* 8: 395–397.

Jia LP, You YZ. 1973. Emaokou stone tool workshop in Huairen. Shanxi (in Chinese). *Kaoguxuebao* 2: 13–26.

Jia LP. 1978. The feature of microlithic and its tradition, origin in China (in Chinese with English abstract). *Vertebrata PalAsiatica* 16: 137–143.

Jia ZX, Zhang XL, Pei SW. 2015. Stone artifacts collected from the Xibaimaying site in the Nihewan Basin (in Chinese). *Acta Anthropologica Sinica* 34: 299–306.

Keates SG. 2007. Microblade technology in Siberia and neighboring regions: an overview. In *Origin and Spread of Microblade Technology in Northern Asia and*

North America, Kuzmin YV, Keates SG, Chen S (eds.). Archaeology Press: Simon Fraser University: Burnaby; 125–146.

Kuzmin YV. 2007. Geoarchaeological aspects of the origin and spread of microblade technology in northern and central Asia. In *Origin and Spread of Microblade Technology in Northern Asia and North America*, Kuzmin YV, Keates SG, Chen S. (eds.). Archaeology Press: Simon Fraser University, Burnaby; 115–124.

Li B, Jacobs Z, Roberts RG. 2016. Investigation of the applicability of standardised growth curves for OSL dating of quartz from Haua Fteah cave, Libya. *Quaternary Geochronology* 35, 1–15.

Lian OB, Roberts RG. 2006. Dating the Quaternary: progress in luminescence dating of sediments. *Quaternary Science Reviews* 25: 2449–2468.

Lisiecki, LE, Raymo ME. 2005. A Pliocene-Pleistocene stack of 57 globally distributed benthic $\delta^{18}O$ records. *Paleoceanography* 20: PA1003.

Liu X, Chi Z, Herzschuh U, Wang Y, Ni J, Xu Q. 2014. A MIS 3 charcoal and pollen record and quantitative precipitation inferences from the Jingerwa section of the Nihewan Basin, north-central China. *Journal of Paleolimnology* 51: 211–221.

Liu Y. 2014. The origin and developmental road of the small tool technology in northern China (in Chinese). *Wenwuchunqiu* 2: 3–13.

Liu Y, Hu YM, Wei Q. 2013. Early to Late Pleistocene human settlements and the evolution of lithic technology in the Nihewan Basin, North China: a macroscopic perspective. *Quaternary International* 295: 204–214.

Mishra S, Chauhan N, Singhvi AK. 2013. Continuity of microblade technology in the Indian subcontinent since 45 ka: implications for the dispersal of modern humans. *PLoS ONE* 8(7): e69280.

Mu H, Xu Q, Zhang S, Hun L, Li M, Li Y, Hu Y, Xie F. 2015. Pollen-based quantitative reconstruction of the paleoclimate during the formation process of Houjiayao Relic Site in Nihewan Basin of China. *Quaternary International* 374: 76–84.

Murray AS, Roberts RG. 1998. Measurement of the equivalent dose in quartz using a regenerative-dose single-aliquot protocol. *Radiation Measurements* 29: 503–515.

Murray AS, Wintle AG. 2000. Luminescence dating of quartz using an improved single-aliquot regenerative-dose protocol. *Radiation Measurements* 32: 57–73.

Murray AS, Wintle AG. 2003. The single-aliquot regenerative-dose protocol: potential for improvements in reliability. *Radiation Measurements* 37: 377–381.

Nian XM, Gao X, Xie F, Mei HJ, Zhou LP. 2014. Chronology of the Youfang site and its implications for the emergence of microblade technology in North China. *Quaternary International* 347: 113–121.

Norton CJ, Gao X. 2008. Hominin–carnivore interactions during the Chinese Early Paleolithic: Taphonomic perspectives from Xujiayao. *Journal of Human Evolution* 55: 164–178.

Preusser F, Degering D, Fuchs M, Hilgers A, Kadereit A, Klasen N, Krbetschek M, Richter D, Spencer JQ. 2008. Luminescence dating: basics, methods and applications. *Eiszeitalter und Gegenwart* 57: 95–149.

Prescott JR, Hutton JT. 1994. Cosmic ray contributions to dose rates for luminescence and ESR dating: large depths and long-term time variations. *Radiation Measurements* 23: 497–500.

Rhodes EJ. 2011. Optically stimulated luminescence dating of sediments over the past 200,000 years. *Annual Review of Earth and Planetary Sciences* 39: 461–488.

Roberts RG, Jacobs Z, Li B, Jankowski NR, Cunningham AC, Rosenfeld AB. 2015. Optical dating in archaeology: thirty years in retrospect and grand challenges for the future. *Journal of Archaeological Science* 56: 41–60.

Roberts RG, Bird M, Olley J, Galbraith R, Lawson E, Laslett G, Yoshida H, Jones R, Fullagar R, Jacobsen G, Hua Q. 1998a. Optical and radiocarbon dating at Jinmium rock shelter in northern Australia. *Nature* 393: 358–362.

Roberts R, Yoshida H, Galbraith R, Laslett G, Jones R, Smith M. 1998b. Single-aliquot and single-grain optical dating confirm thermoluminescence age estimates at Malakunanja II rock shelter in northern Australia. *Ancient TL* 16: 19–24.

Schick K, Toth N, Qi W, Clark JD, Etler D. 1991. Archaeological perspectives in the Nihewan Basin, China. *Journal of Human Evolution* 21: 13–26.

Teihard de Chardin P, Pei WG. 1932. The lithic industry of the Sinanthropus deposits in Choukoutien. *Bulletin of the Geological Society of China* 11: 315–364.

Teihard de Chadin TD, Licent F. 1924. On the discovery of a Palaeolithic industry in northern China. *Bulletin of the Geological Society of China* 3: 45–50.

Tu H, Shen GJ, Li HX, Xie F, Granger DE. 2015. $^{26}Al/^{10}Be$ Burial Dating of Xujiayao-Houjiayao Site in Nihewan Basin, Northern China. *PLoS ONE* 10(2): e0118315.

Wang H, Deng C, Zhu R, Wei Q, Hou Y, Boëda E. 2005. Magnetostratigraphic dating of the Donggutuo and Maliang Paleolithic sites in the Nihewan Basin, North China. *Quaternary Research* 64: 1–11.

Wang YP. 2006. *Stone Artefacts Studies: Explorations of the Palaeolithic Archaeological Methods* (in Chinese). Peking University Press: Beijing.

Wei Q. 2004. The Paleolithic of Nihewan Basin (in Chinese). In *Review of China's Century of Archaeological Research (Paleolithic Archaeology)*, Lu ZE (ed). Science Press: Beijing; 84–110.

Wei Q, Pei SW, Jia ZX, Chi ZQ, Wang Y. 2016. Heitugou Paleolithic site from the Lower Pleistocence in the Nihewan Basin, northern China (in Chinese with English abstract). *Acta Anthropologica Sinica* 35: 43–62.

Wintle AG. 2014. Luminescence dating methods. In *Treatise on Geochemistry (2nd edition)*, Holland H, Turekian K (eds.). Elsevier: Oxford; 17–35.

Wintle AG, Murray AS. 2006. A review of quartz optically stimulated luminescence characteristics and their relevance in single-aliquot regeneration dating protocols. *Radiation Measurements* 41: 369–391.

Xia ZK, Chen FY, Chen G, Zheng GW, Xie F, Mei HJ. 2001. Environmental background of evolution from the Paleolithic to Neolithic culture in Nihewan Basin, North China. *Science in China Series D: Earth Sciences* 44: 779–788.

Xie F, Li J, Liu LQ. 2006. *Paleolithic Archeology in the Nihewan Basin* (in Chinese). Huashan Literature and Arts Press: Shijiazhuang.

Xie F, Yu SF. 1989. A study of Paleolithic remains from Xibaimaying, Yangyuan, Hebei (in Chinese with English abstract). *Wenwu Chunqiu* 3: 13–26.

Yi MJ, Gao X, Li F, Chen F. 2016. Rethinking the origin of microblade technology: A chronological and ecological perspective. *Quaternary International* 400: 130–139.

Yuan SX. 1993. AMS radiocarbon dating of Xinglong carved antler, Shiyu and Ximiao sites (in Chinese with English abstract). *Acta Anthroplogica Sinica* 12: 92–95.

Zhang CC, Li L, Wang J, Xu QH, Huang HF. 2015. Research on the relationship between the old river and living environment for ancient human at Houjiayao site, Yangyuan County, Hebei Province (in Chinese with English abstract). *Quaternary Sciences* 35: 733–741.

Zhang JF, Wang XQ, Qiu WL, Shelach G, Hu G, Fu X, Zhuang MG, Zhou LP. 2011. The paleolithic site of Longwangchan in the middle Yellow River, China: chronology, paleoenvironment and implications. *Journal of Archaeological Science* 38: 1537–1550.

Zhang SS. 1990. Regional industrial gradual advance and cultural exchange of Paleolithic in North China (in Chinese with English abstract). *Acta Anthroplogica Sinica* 9: 322–333.

Zhang SS. 1999. On the important advancements of the Palaeolithic archeology in China since 1949 (in Chinese with English abstract). *Acta Anthroplogica Sinica* 18: 193–214.

Zhao H, Lu Y, Wang C, Chen J, Liu J, Mao H. 2010. ReOSL dating of aeolian and fluvial sediments from Nihewan Basin, northern China and its environmental application. *Quaternary Geochronology* 5: 159–163.

Zhu RX, Hoffman KA, Potts R, Deng CL, Pan YX, Guo B, Shi CD, Guo ZT, Yuan BY, Hou YM, Huang WW. 2001. Earliest presence of humans in northeast Asia. *Nature* 413: 413–417.

Zhu RX, Potts R, Xie F, Hoffman KA, Deng CL, Shi CD, Pan YX, Wang HQ, Shi RP, Wang YC, Shi GH. 2004. New evidence on the earliest human presence at high northern latitudes in northeast Asia. *Nature* 431: 559–562.

Zhu ZY. 2006. The study on lithic assemblage from the Hutouliang site in North China (in Chinese with English abstract). PhD thesis, Institute of Vertebrate Paleontology and Paleoanthropology, Chinese Academy of Sciences: Beijing.

Figure captions

Fig. 1: (a) Map of China showing the Palaeolithic sites mentioned in this study (modified after Han et al., 2012). Triangles and circles represent small-tool and microlithic sites, respectively. (b) Map of the Nihewan Basin showing the Palaeolithic sites mentioned in this study (modified after Wei, 2004). Zhiyu has artefacts 'transitional' between small-tool and microlithic technologies (Jia et al., 1972; Jia, 1978).

Fig. 2: (a) Photo looking northwest, showing the location of the Xibaimaying site on the east bank of the Nangou gully. (b) Sedimentary profile of the excavated east face, showing locations of the OSL samples. (c) Animal remains in the cultural layer, from which OSL sample XBMY-OSL-1 was collected. (d) Schematic of the excavated sedimentary profile, with OSL sample positions and ages.

Fig. 3: Typical artefacts from the Xibaimaying site (Xie and Yu, 1989; Xie et al., 2006): (a)–(e) scrapers, (f) and (g) points, (h) flake, (i) and (j) hammered core, (k) and (l) percussion core, (m) bone tool.

Fig. 4: (a) Typical OSL decay curve and (b) dose response curve for a single grain of quartz from sample XBMY-OSL-1. The dose response curves are fitted using a single saturating exponential function of the form $I = I_0(1 - e^{-D/D_0}) + c$, where I is the sensitivity-corrected OSL intensity, D is the regenerative dose, D_0 is the characteristic saturation dose, and I_0 and c define the saturation value of the exponential curve. The D_e is obtained by projecting the sensitivity-corrected natural OSL signal (the upper point on the y-axis) on to the fitted curve and interpolating the dose (dashed line).

Fig. 5: Results of the preheat temperature test on sample XBMY-OSL-5, conducted using the single-aliquot regenerative-dose procedure in Table S1a. The D_e values and corresponding recycling and recuperation ratios are plotted as a function of preheat temperature in (a), (b) and (c), respectively. Each data point represents the weighted mean for 13–20 aliquots and the vertical bars indicate the corresponding 1σ errors.

Fig. 6: (a) Distribution of measured (recovered) doses for all accepted grains in the dose recovery test on sample XBMY-OSL-1, expressed as the ratio of recovered dose to given dose (140 Gy). Open circles and closed triangles denote grains with D_0 values of less than and more than 120 Gy (the optimum-D_0 threshold; see Table S3), respectively. The grey band is centred on the weighted mean ratio (0.97 ± 0.04) for the grains above the optimum-D_0 threshold of 120 Gy, calculated using the CAM, which was also used to estimate the over-dispersion (OD) among the individual recovered doses. (b) Mean dose recovery ratios (recovered dose/given dose) (red squares) and the corresponding number of accepted grains (grey triangles) for sample XBMY-OSL-1 plotted as a function of the D_0 threshold value. Ratios are statistically consistent (at 2σ) with unity for all D_0 thresholds higher than 90 Gy.

Fig. 7: (a)–(d) D_e distributions for the accepted grains of samples XBMY-OSL-1, -2, -3 and -5, respectively. Open circles and closed triangles denote D_e values for grains with D_0 values below and above the optimum-D_0 thresholds, respectively. The grey bands are centred on the weighted mean D_e values for the grains at and above the optimum-D_0 thresholds.

Fig. 8: Weighted mean (CAM) D_e estimates (red squares) and the corresponding number of accepted grains (grey triangles) plotted as a function of the D_0 threshold

value. The dashed lines indicate the CAM D_e values at the optimum-D_0 threshold for each sample (150, 150, 120 and 30 Gy for samples XBMY-OSL-1, -2, -3 and -5, respectively).

Fig. 9: Comparison of approximate ages reported previously for small-tool and microlithic sites in the Nihewan Basin and the OSL ages obtained in this study for the Xibaimaying site. The vertical grey band indicates the prevailing view that the small-tool and microblade industries coexisted during the Upper Palaeolithic in the Nihewan Basin, based on U-series dating of bovid teeth at Xiabimaying. The OSL ages for Xibaimaying reported here imply a developmental trend from small-tool technology (mid-MIS 3) to ‘transitional’ small/microlithic (Zhiyu, late MIS 3) to typical microlithic technology (Youfang, early MIS 2) in the Nihewan Basin, denoted by the dashed arrows. The oxygen isotope ($\delta^{18}O$) curve and Marine Isotope Stage (MIS) boundaries follow Lisiecki and Raymo (2005). The age range of the Yujiagou site is based on thermoluminescence (TL) dating of fine-grained quartz (Xia et al., 2001).

Table 1. Dose rates, D_e values and OSL ages for quartz grains from the Xibaimaying site.

Sample	Depth, m	Grain size, μm	Water, % [a]	U, ppm	Th, ppm	K, %	Environmental dose rate, Gy/ka [b]				D_e, Gy [c]	Age, ka
							Gamma	Beta	Cosmic	Total		
XBMY-OSL-1	2.8	125–150	15 ± 5	3.44 ± 0.15	10.99 ± 1.23	1.98	1.20 ± 0.08	1.82 ± 0.12	0.15 ± 0.03	3.21 ± 0.16	147.2 ± 7.5 (n = 89)	46 ± 3
XBMY-OSL-2	2.5	125–150	10 ± 3	4.15 ± 0.16	10.55 ± 1.22	2.02	1.33 ± 0.07	2.04 ± 0.08	0.17 ± 0.04	3.56 ± 0.12	112.4 ± 6.5 (n = 74)	32 ± 2
XBMY-OSL-3	2.0	125–150	10 ± 3	4.21 ± 0.17	9.74 ± 1.31	1.85	1.26 ± 0.07	1.96 ± 0.08	0.18 ± 0.04	3.42 ± 0.12	82.7 ± 7.5 (n = 32)	24 ± 2
XBMY-OSL-5	0.5	125–150	10 ± 3	3.67 ± 0.14	8.03 ± 1.04	1.61	1.08 ± 0.06	1.65 ± 0.07	0.20 ± 0.05	2.96 ± 0.10	39.3 ± 2.5 (n = 76)	13 ± 1

[a] Time-averaged water contents for fluvial sample XBMY-OSL-1 and colluvial/aeolian samples XBMY-OSL-2, 3 and 5.

[b] Dose rates corrected for water attenuation. The total dose rate also includes an internal dose rate of 0.03 ± 0.01 Gy/ka.

[c] A systematic error of 2% has been added in quadrature to the D_e measurement error to allow for possible bias in the calibration of the laboratory beta source. The values in parentheses (n) indicate the number of the final accepted grains with D_0 values at and above the optimum-D_0 threshold.

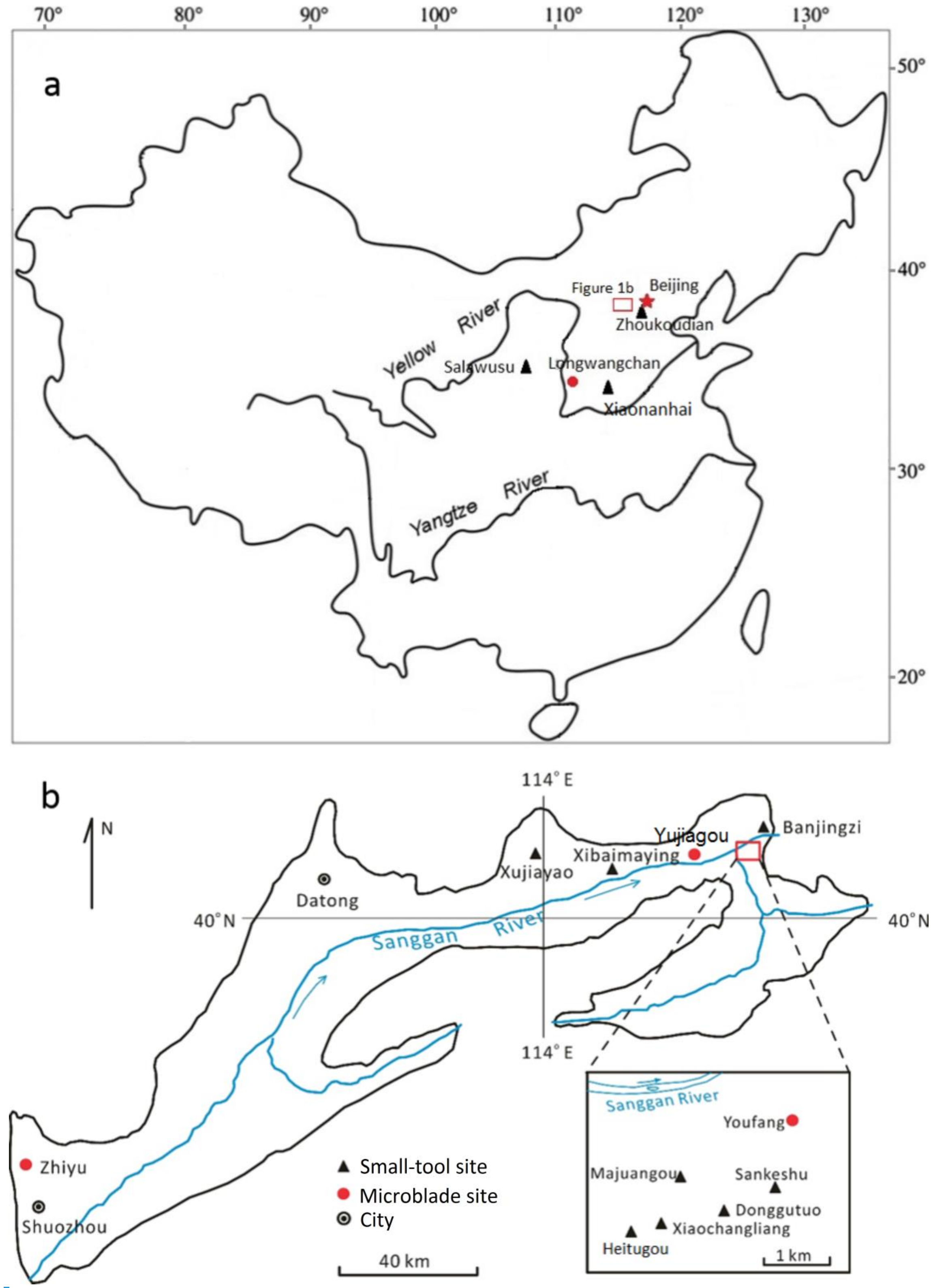

70°
80°
90°
100°
110°
120°
130°
50°
40°
30°
20°
a
Figure 1b
Beijing
Zhoukoudian
Yellow River
Salawusu
Longwangchan
Xiaonanhai
Yangtze River
b
N
114° E
Banjingzi
Yujiagou
Xibaimaying
Xujiayao
Datong
40° N
40° N
Sanggan River
114° E
Sanggan River
Youfang
Majuangou
Sankeshu
Donggutuo
Xiaochangliang
Heitugou
1 km
Zhiyu
Shuozhou
Small-tool site
Microblade site
City
40 km

Fig. 1

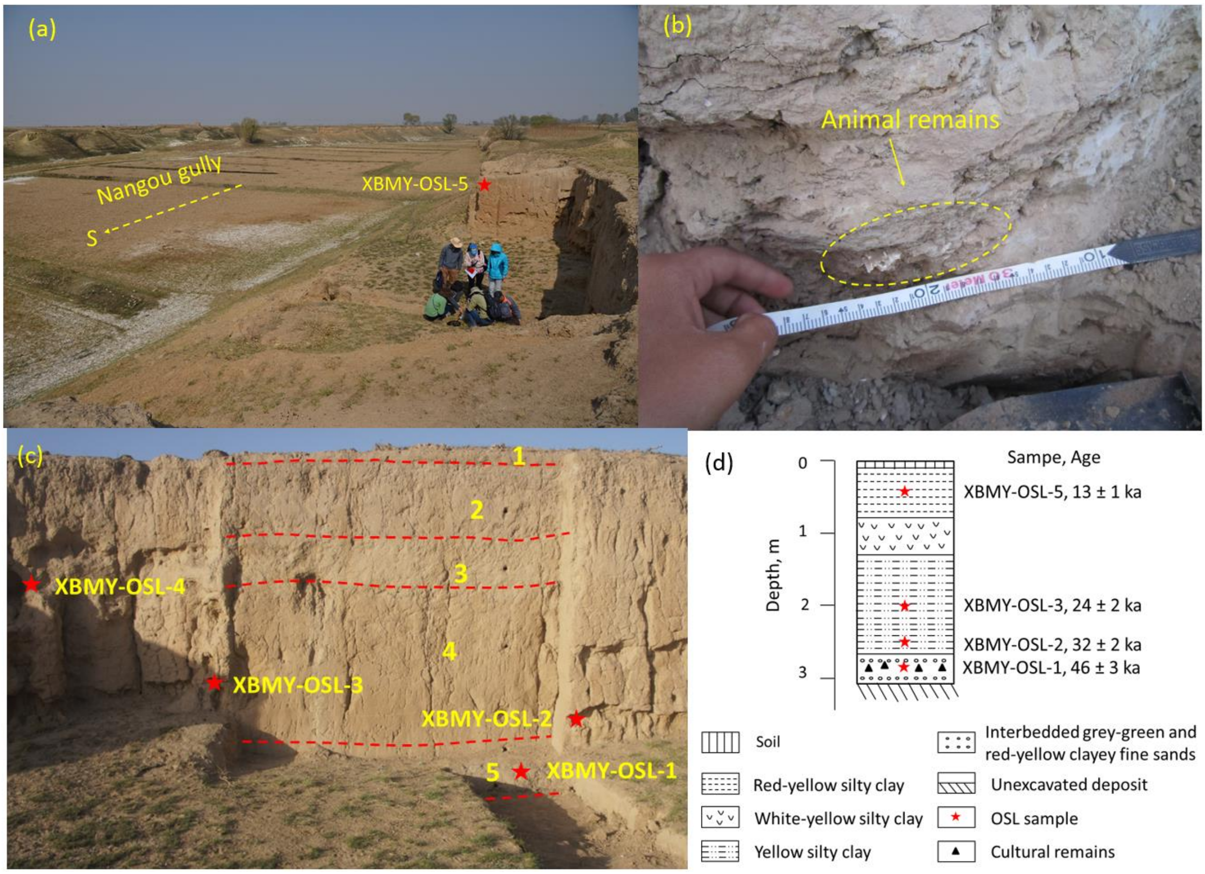
(a)
Nangou gully
S
XBMY-OSL-5
(b)
Animal remains
(c)
1
2
3
4
5
XBMY-OSL-4
XBMY-OSL-3
XBMY-OSL-2
XBMY-OSL-1
(d)
Sampe, Age
Depth, m
0
1
2
3
XBMY-OSL-5, 13 ± 1 ka
XBMY-OSL-3, 24 ± 2 ka
XBMY-OSL-2, 32 ± 2 ka
XBMY-OSL-1, 46 ± 3 ka
Soil
Red-yellow silty clay
White-yellow silty clay
Yellow silty clay
Interbedded grey-green and red-yellow clayey fine sands
Unexcavated deposit
OSL sample
Cultural remains

Fig. 2

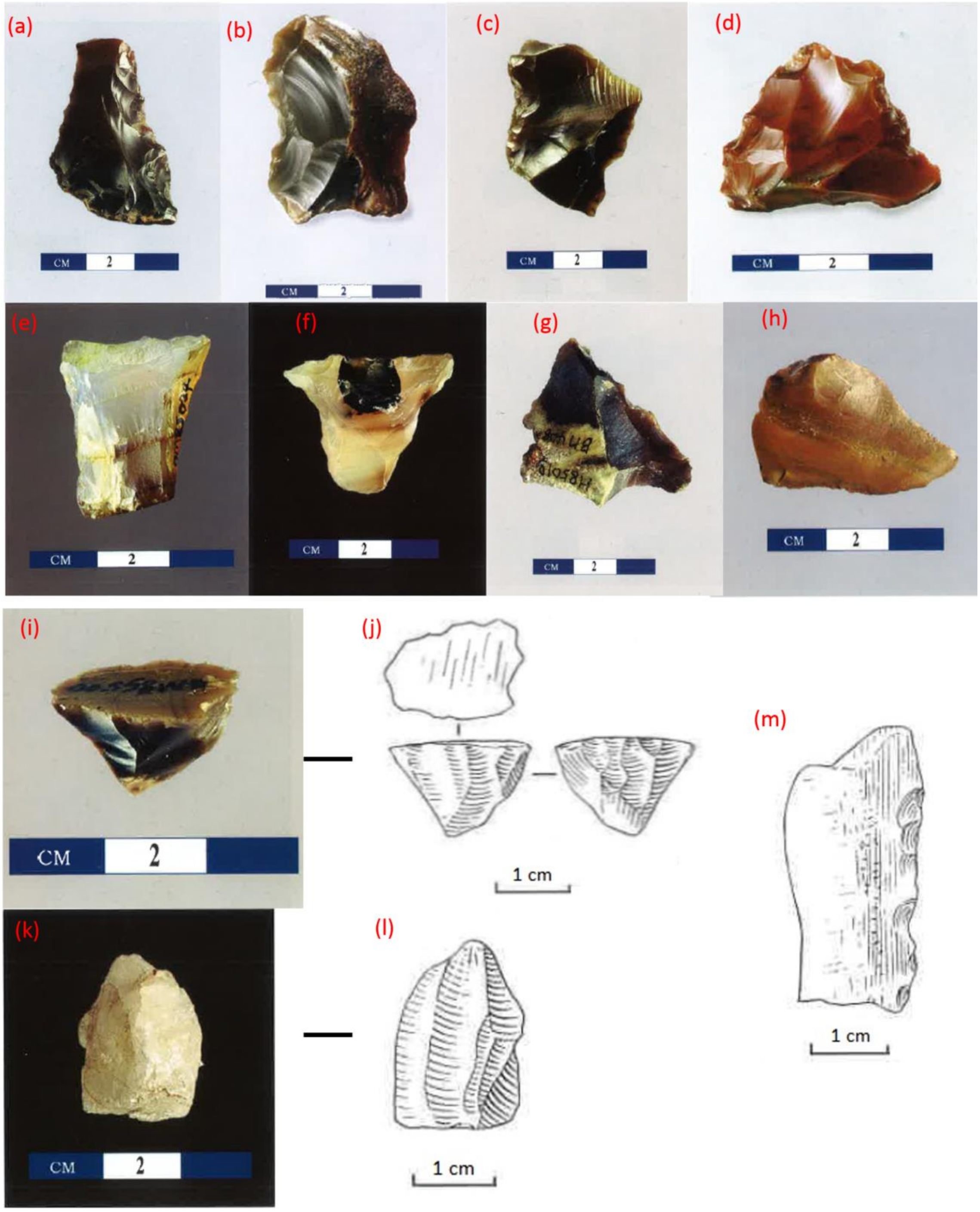

Fig. 3

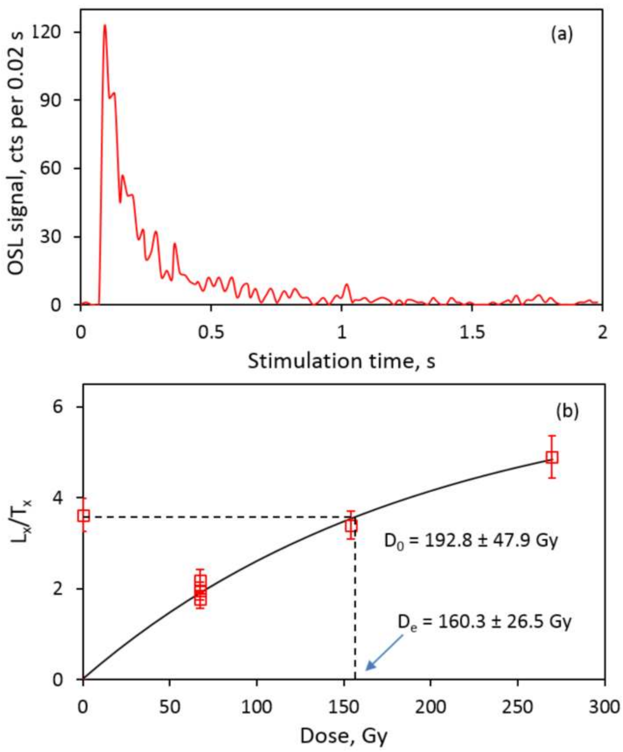

(a)
OSL signal, cts per 0.02 s
0
30
60
90
120
0
0.5
1
1.5
2
Stimulation time, s
(b)
L_x/T_x
0
2
4
6
D_0 = 192.8 ± 47.9 Gy
D_e = 160.3 ± 26.5 Gy
0
50
100
150
200
250
300
Dose, Gy

Fig. 4

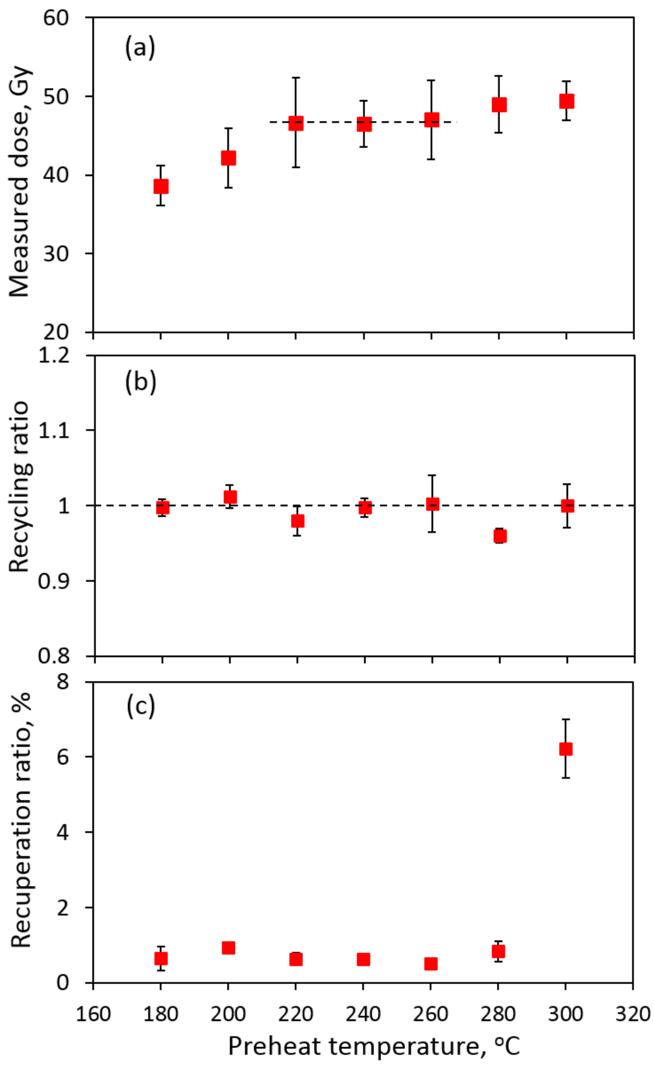

(a)
Measured dose, Gy
60
50
40
30
20
(b)
Recycling ratio
1.2
1.1
1
0.9
0.8
(c)
Recuperation ratio, %
8
6
4
2
0
160
180
200
220
240
260
280
300
320
Preheat temperature, °C

Fig. 5

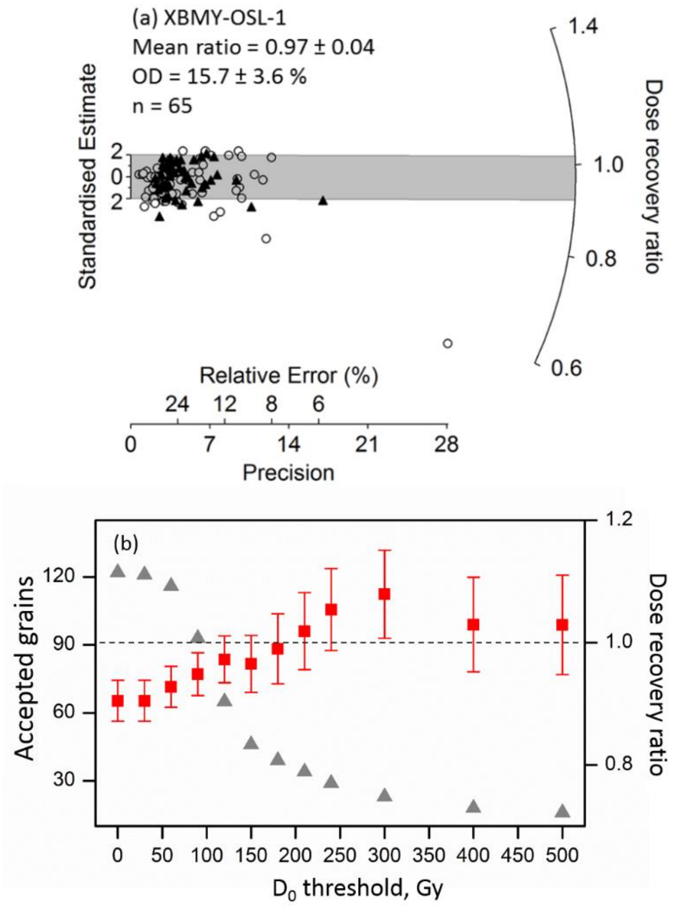

(a) XBMY-OSL-1
Mean ratio = 0.97 ± 0.04
OD = 15.7 ± 3.6 %
n = 65
Standardised Estimate
2
0
2
Dose recovery ratio
1.4
1.0
0.8
0.6
Relative Error (%)
24
12
8
6
0
7
14
21
28
Precision
(b)
Accepted grains
120
90
60
30
Dose recovery ratio
1.2
1.0
0.8
0
50
100
150
200
250
300
350
400
450
500
D0 threshold, Gy

Fig. 6

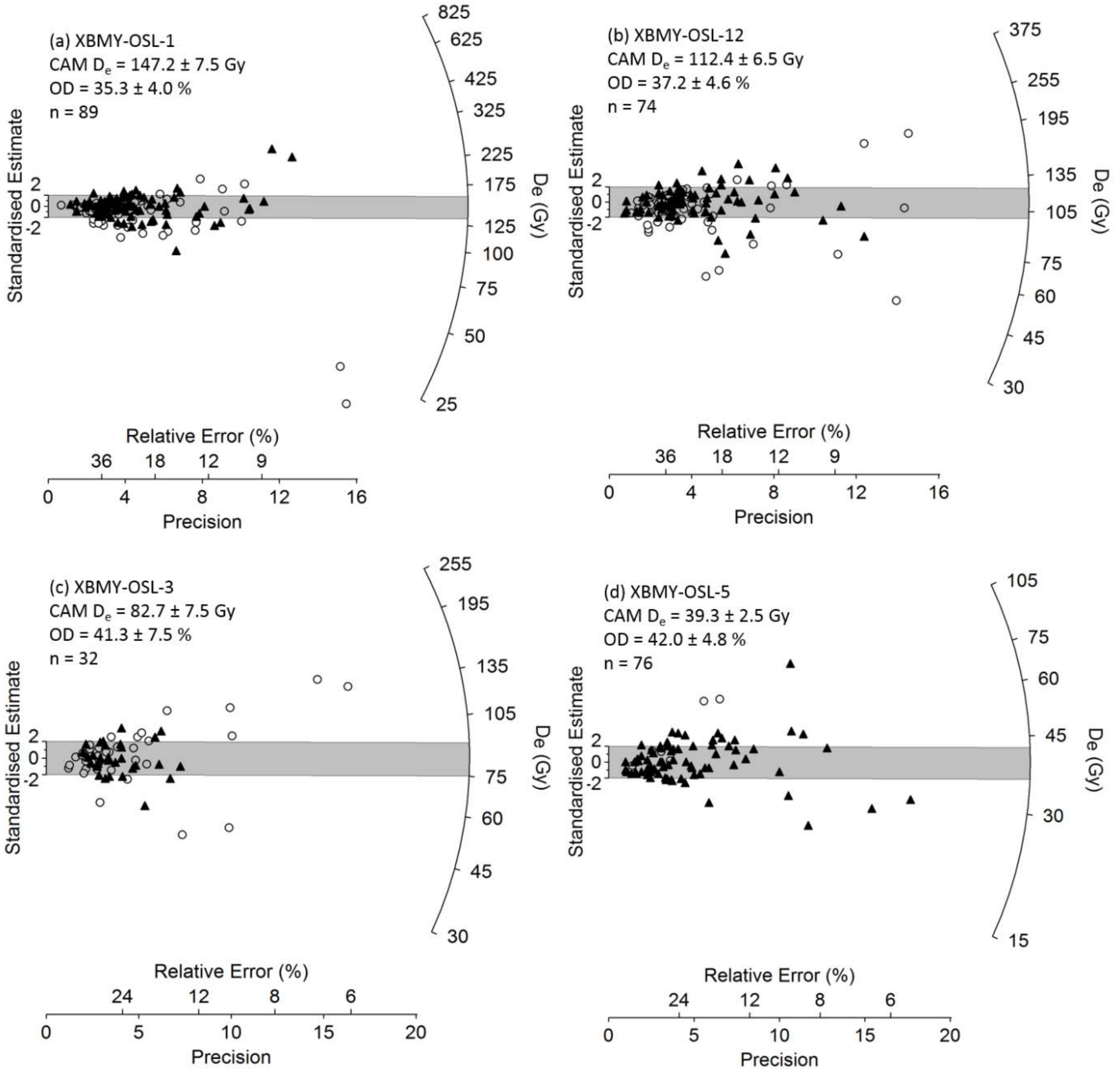

(a) XBMY-OSL-1
CAM De = 147.2 ± 7.5 Gy
OD = 35.3 ± 4.0 %
n = 89
Standardised Estimate
De (Gy)
Relative Error (%)
Precision
(b) XBMY-OSL-12
CAM De = 112.4 ± 6.5 Gy
OD = 37.2 ± 4.6 %
n = 74
(c) XBMY-OSL-3
CAM De = 82.7 ± 7.5 Gy
OD = 41.3 ± 7.5 %
n = 32
(d) XBMY-OSL-5
CAM De = 39.3 ± 2.5 Gy
OD = 42.0 ± 4.8 %
n = 76

Fig. 7

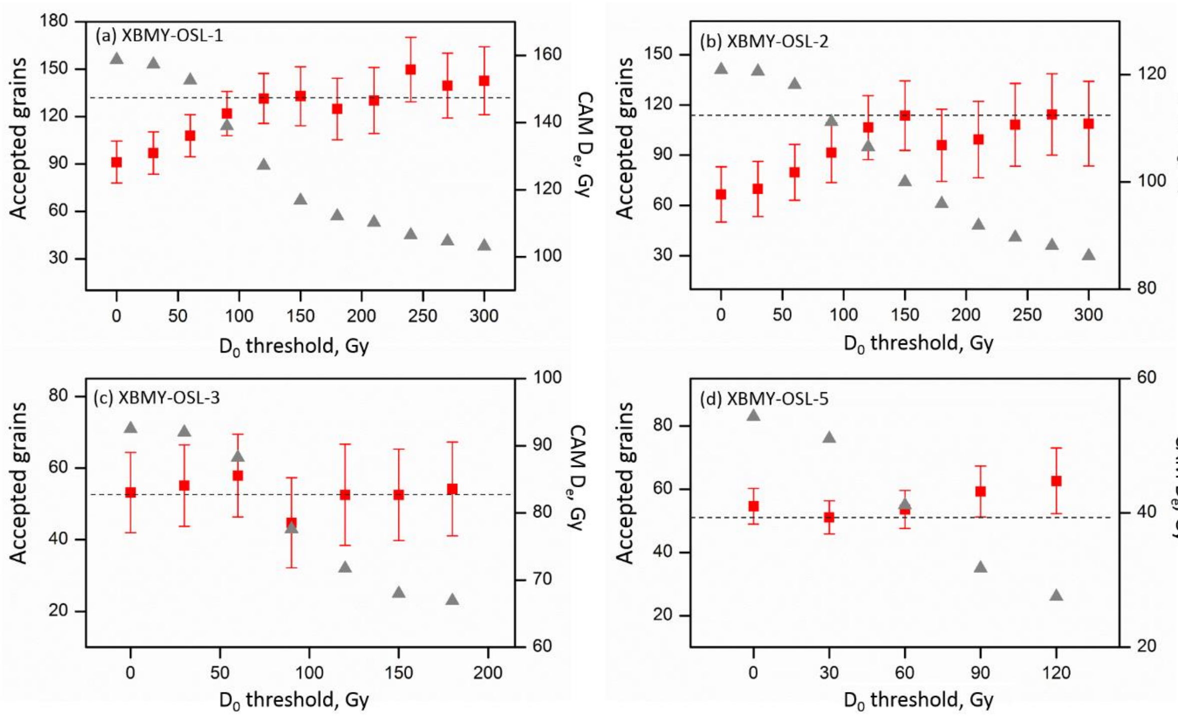

(a) XBMY-OSL-1
Accepted grains
CAM De, Gy
D0 threshold, Gy
(b) XBMY-OSL-2
Accepted grains
CAM De, Gy
D0 threshold, Gy
(c) XBMY-OSL-3
Accepted grains
CAM De, Gy
D0 threshold, Gy
(d) XBMY-OSL-5
Accepted grains
CAM De, Gy
D0 threshold, Gy

Fig. 8

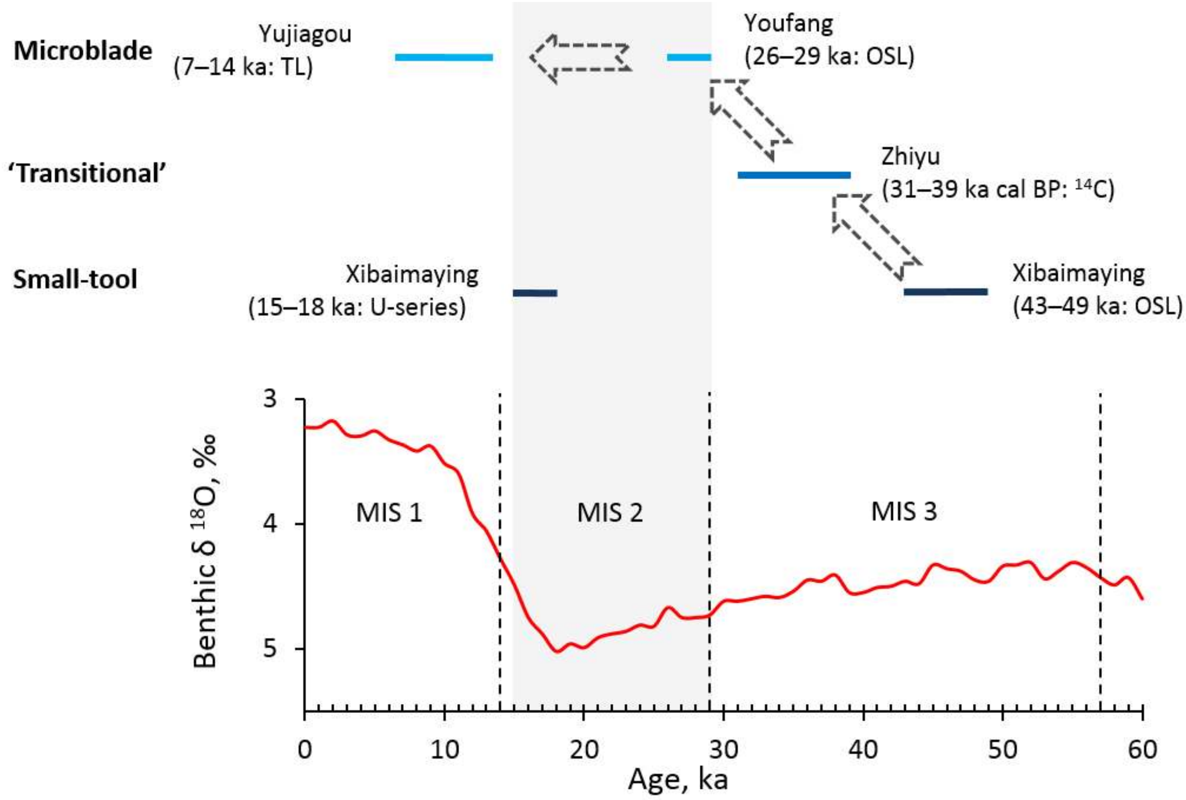
Microblade
Yujiagou
(7–14 ka: TL)
Youfang
(26–29 ka: OSL)
'Transitional'
Zhiyu
(31–39 ka cal BP: 14C)
Small-tool
Xibaimaying
(15–18 ka: U-series)
Xibaimaying
(43–49 ka: OSL)
Benthic δ 18O, ‰
3
4
5
MIS 1
MIS 2
MIS 3
0
10
20
30
40
50
60
Age, ka

Fig. 9

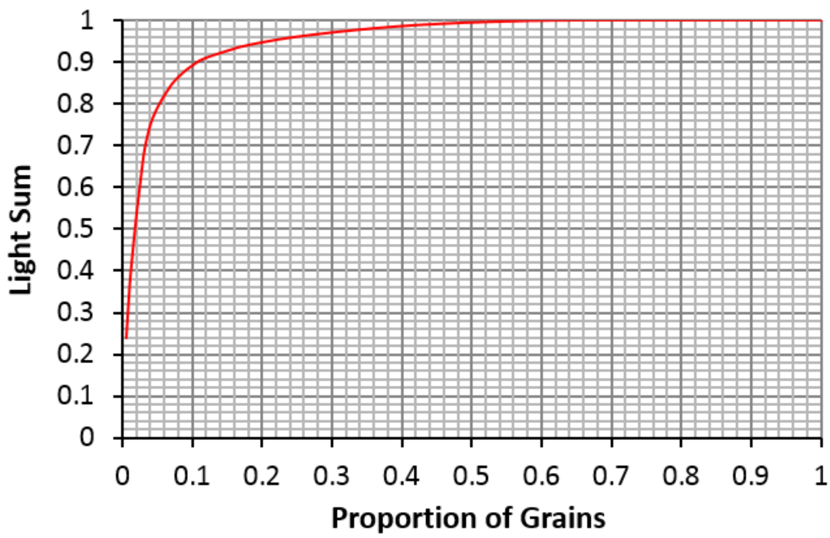

Figure S1 The single-grain ‘brightness’ distribution for 200 individual grains of sample XBMY-OSL-1. The cumulative light sum of the T_n signals (shown on the *y*-axis) is plotted as a function of the corresponding proportion of grains (shown on the *x*-axis).

Table S1 The single-aliquot regenerative-dose (SAR) procedures used in this study (based on Galbraith et al., 1999; Murray and Wintle, 2000, 2003).

(a) Single-aliquot procedure: preheat temperature test [a]		
Step	Treatment	Signal
1 [b]	Give regenerative dose, D_i	
2	Heat at 180–300 °C for 10 s	
3	Measure OSL at 125 °C for 40 s	L_n, L_x
4	Give test dose, D_t	
5	Heat at 20–40 °C lower than step 2 for 10 s	
6	Measure OSL at 125 °C for 40 s	T_n, T_x
7 [c]	Bleach at 20 °C higher than step 2 for 40 s	
8	Return to step 1	
(b) Single-grain procedure: dose recovery test and D_e estimation [d]		
Step	Treatment	Signal
1 [b]	Give regenerative dose, D_i	
2	Heat at 240 °C for 10 s	
3	Measure OSL at 125 °C for 1–2 s	L_n, L_x
4	Give test dose, D_t	
5	Heat at 200 °C for 10 s	
6	Measure OSL at 125 °C for 1–2 s	T_n, T_x
7 [c]	Bleach at 260 °C for 40 s	
8	Return to step 1	

[a] The single-aliquot procedure was used to conduct a preheat temperature test on sample XBMY-OSL-5. The test dose preheat (step 5) was set 40 °C lower than the preheat applied to the natural and regenerative doses in step 2, except for the 180 °C preheat in step 2 which was accompanied by a test dose preheat of 160 °C in step 5.

[b] For the natural dose, i = 0 and D_i = 0 Gy. The OSL signals induced by stimulation of the natural dose and its corresponding test dose are denoted L_n and T_n respectively, and the OSL signals induced by stimulation of the regenerative doses and their corresponding test doses are denoted L_x and T_x, respectively. The entire sequence is repeated for several regenerative doses, including a zero dose and a duplicate dose, to monitor the extent of recuperation and to determine the recycling ratio, respectively.

[c] The 'hot optical bleach' in step 7 consists of OSL stimulation using blue light-emitting diodes with the sample held at a temperature 20 °C higher than the corresponding preheat in step 2.

[d] A further (triplicate) regenerative dose cycle was included at the end of the single-grain SAR sequence to check for feldspar contamination of individual quartz grains on the basis of their OSL IR depletion ratios (Duller, 2003). The regenerative dose was stimulated using infrared light-emitting diodes for 40 s at 50 °C prior to stimulation of the OSL signal using a green laser.

Table S2 Number of individual quartz grains measured, rejected and accepted for D_e determination, and the reasons for their rejection.

Sample	No. of grains measured	Weak T_n signal [a] or test dose error >25% [b]	Recuperation ratio >10% [c]	Poor recycling ratio or OSL IR depletion ratio [d]	Poor DRC fit to L_x/T_x [e]	L_n/T_n consistent with or above saturation [f]	Sum of rejected grains	No. of grains accepted for D_e estimation
dose recovery test [g]	2000	1715	11	101	2	49	1878	122
XBMY-OSL-1	3400	3066	9	118	5	46	3244	156
XBMY-OSL-2	2800	2492	63	53	10	41	2659	141
XBMY-OSL-3	1400	1267	23	28	2	9	1329	71
XBMY-OSL-5	1900	1738	17	60	0	2	1815	83

[a] Initial 0.12 s of the T_n signal is less than 3 times the corresponding background (determined from the last 0.12 s of stimulation).

[b] Relative error on the T_n signal exceeds 25%.

[c] Extent of recuperation (ratio of zero dose L_x/T_x signal to the L_n/T_n signal, expressed as a percentage) exceeds 10%.

[d] Recycling ratio or the OSL IR depletion ratio differs from unity by more than 2σ.

[e] DRC is an obviously poor fit to the L_x/T_x data points.

[f] L_n/T_n signal consistent with or exceeding the saturation level of the corresponding DRC (i.e., does not intersect the DRC), and, hence, no finite estimate of D_e can be obtained.

[g] Conducted on sample XBMY-OSL-1.

Table S3 Central Age Model (CAM) D_e values, over-dispersion values, and number of accepted and saturated grains at various characteristic saturation dose (D_0) thresholds. The optimum-D_0 threshold values are highlighted in bold.

Sample	D_0 threshold (Gy)	No. of grains with L_n/T_n values consistent with or above saturation	No. of grains used for D_e estimation	CAM D_e (Gy)	Over-dispersion (%)
XBMY-OSL-1 dose recovery test	0	49	122	126.7 ± 4.7	23.5 ± 2.9
	30	35	121	126.7 ± 4.7	23.5 ± 2.9
	60	20	116	129.9 ± 4.7	21.4 ± 2.9
	90	8	93	132.8 ± 4.9	18.5 ± 3.1
	120	**0**	**65**	**136.2 ± 5.3**	**15.7 ± 3.6**
	150		46	138.6 ± 8.0	19.3 ± 4.4
	180		39	142.6 ± 8.8	23.1 ± 5.3
	210		34	145.1 ± 8.4	22.3 ± 6.0
	240		29	147.6 ± 9.3	18.9 ± 6.9
	300		23	151.1 ± 10.1	16.1 ± 7.9
	400		18	144.1 ± 10.8	17.8 ± 8.3
	500		16	144.1 ± 11.4	18.6 ± 8.4
XBMY-OSL-1	0	46	156	128.2 ± 6.2	47.4 ± 3.6
	30	40	153	130.9 ± 6.3	45.9 ± 3.5
	60	19	143	136.1 ± 6.2	40.9 ± 3.4
	90	4	114	142.6 ± 6.6	36.1 ± 3.5
	120	**0**	**89**	**147.2 ± 7.5**	**35.3 ± 3.9**
	150		67	147.8 ± 8.8	38.2 ± 4.7
	180		57	144.0 ± 9.1	37.6 ± 5.1
	210		53	146.6 ± 9.8	38.4 ± 5.4
	240		45	155.8 ± 9.6	29.5 ± 5.3
	270		41	151.0 ± 9.7	29.2 ± 5.5
	300		38	152.4 ± 10.1	29.3 ± 5.7
	0	41	141	97.7 ± 5.2	48.4 ± 4.0

XBMY-OSL-2	30	37	140	98.7 ± 5.1	47.4 ± 3.9
	60	24	132	101.8 ± 5.2	44.3 ± 3.9
	90	9	110	105.5 ± 5.6	41.7 ± 4.1
	120	2	95	110.2 ± 6.0	39.4 ± 4.2
	150	**0**	**74**	**112.4 ± 6.5**	**37.2 ± 4.6**
	180		61	106.8 ± 6.7	37.3 ± 5.0
	210		48	107.9 ± 7.1	33.9 ± 5.5
	240		41	110.7 ± 7.7	32.9 ± 5.8
	270		36	112.6 ± 7.6	27.5 ± 6.0
	300		30	110.9 ± 7.9	25.4 ± 6.7
XBMY-OSL-3	0	9	71	83.0 ± 5.6	49.6 ± 5.6
	30	6	70	84.1 ± 5.6	49.2 ± 5.6
	60	4	63	85.5 ± 5.7	46.5 ± 5.7
	90	1	43	78.5 ± 6.9	45.6 ± 6.9
	120	**0**	**32**	**82.7 ± 7.5**	**41.3 ± 7.5**
	150		25	82.7 ± 7.3	29.8 ± 7.3
	180		23	83.6 ± 7.5	28.5 ± 7.5
	210		17	79.5 ± 8.6	27.4 ± 8.6
XBMY-OSL-5	0	2	83	41.0 ± 2.7	46.4 ± 4.9
	30	**0**	**76**	**39.3 ± 2.5**	**42.0 ± 4.8**
	60		55	40.5 ± 2.8	39.3 ± 5.5
	90		35	43.2 ± 3.8	40.4 ± 7.2
	120		26	44.8 ± 4.9	45.3 ± 8.9